Theory for Hydrogen Desorption in Ferritic Steel

Eun Ju Song [a] Dong-Woo Suh [a] H. K. D. H. Bhadeshia [a,b]

[a] *Graduate Institute of Ferrous Technology, POSTECH, Republic of Korea*
[b] *Materials Science and Metallurgy, University of Cambridge, U.K.*

Abstract

After a concise review of the analytical models available for the interpretation of thermal desorption rates for hydrogen effusion from steel, a numerical method that incorporates the essence of local equilibrium and detrapping kinetics has been implemented to account for the real complexity of practical experiments. For example, the model permits the treatment of multiple kinds of traps, uses very few fitting parameters, and has been tested against new experimental data and to assess the influence of a variety of variables such as trap density, on the nature of the desorption process. There remain, however, significant discrepancies when attempts are made to rationalise diverse observations reported in the literature. In particular, comparisons made between the trapping of hydrogen in pure iron and interstitial-free steel indicate a much stronger binding energy for hydrogen in the former case.

Key words: hydrogen trapping, thermal desorption spectra, dislocations, grain boundaries

1 Introduction

Hydrogen is a pernicious solute in iron in the sense that it leads to dramatic changes in the ability of the metal to absorb energy during fracture, at concentrations which are so small that it is difficult to avoid the ingress of nascent hydrogen during, for example, corrosion reactions. Studies of hydrogen embrittlement tend to be of two kinds, the first to characterise the potency of embrittlement, and the second relatively recent approach, to render it innocuous should it enter the steel [1–4].

Email address: `dongwoo1@postech.ac.kr` (Dong-Woo Suh).

It is established that the passage of hydrogen through a steel is hindered by lattice imperfections which tend to attract and bind it, thus rendering it immobile at temperatures where it should normally be able to diffuse readily [5]. This phenomenon, known as *trapping*, can be investigated using thermal desorption spectroscopy (TDS) which monitors the rate at which hydrogen is released from a sample during continuous heating. Strong traps release their hydrogen at higher temperatures and data such as these can be used to probe the parameters defining the interaction of hydrogen with defects. The technique is nevertheless indirect so the interpretation of the curve of desorption rate versus temperature and heating rate requires interpretation, and as will be seen later, there are difficulties with current methods. The methods and their limitations are reviewed first, and aspects of the available theory are then incorporated into a new numerical model which permits more complex problems to be resolved, for example the role of multiple trapping centres. The method is then validated using new experimental data and an assessment of published data from the literature.

2 Models

2.1 Reaction Kinetics Model

Kissinger proposed a generic model for differential thermal analysis covering reactions of any order $m = 1, 2, \ldots$, where m describes the relationship between the measured rate dx/dt and unreacted material $(1 - x)^m$ [6]. In this respect the model is akin to chemical reaction rate theory [7]. In its first order form, the theory has been applied to hydrogen desorption by Choo and Lee [8] in order to calculate a detrapping activation energy E_a:

$$\frac{dx}{dt} = A(1 - x) \exp\left\{\frac{-E_a}{RT}\right\} \quad \text{with} \quad x = \frac{H_0 - H_t}{H_0} \tag{1}$$

where H_0 and H_t are the original and instantaneous hydrogen concentrations in the sample, so that x is the fraction of hydrogen released, A is a proportionality constant, R is the gas constant, T is the absolute temperature, and t the time. For a constant heating rate, ϕ, the maximum desorption rate is obtained by setting the derivative of equation 1 to zero, thus yielding the relationship:

$$\frac{\partial \ln\{\phi/T_p^2\}}{\partial\{1/T_p\}} = \frac{-E_a}{R} \tag{2}$$

where T_p is the temperature corresponding to the maximum hydrogen desorption rate. It follows that the activation energy can be deduced by plotting $\ln\{\phi/T_p^2\}$ against $1/T_p$ for a variety of heating rates. Much research has been

2

carried out using this method [9–12]. However, the model is based on chemical reaction kinetics and deals with homogeneous reactions, whereas the experiments involve the diffusion of hydrogen toward the sample surface. It does not contain information about the size or shape of the sample, and does not apply when the rate limiting step is diffusion rather than detrapping, as can be the case for example for hydrogen effusion from austenite.

2.2 Diffusion & Trapping

A model which accounts for the capture and release of hydrogen from traps, and diffusion through the lattice, was proposed by McNabb and Foster [13]. Their analytical equations can be adapted to finite difference schemes so that the real complexity associated with experiments can be properly dealt with, for example, an arbitrary initial distribution of hydrogen [14]. If θ_t is defined as the occupancy of trap sites by hydrogen atoms,

$$\frac{d\theta_t}{dt} = kC_l(1 - \theta_t) - p\theta_t \qquad \text{where} \qquad \theta_t = \frac{C_t}{N_t} \qquad (3)$$

where N_t is the density of traps, C_l and C_t are the hydrogen concentrations in lattice and trap sites respectively, and k and p represent the rates of trapping and escaping, respectively:

$$k = k_0 \exp\left\{\frac{-Q_D}{RT}\right\} \qquad \text{and} \qquad p = p_0 \exp\left\{\frac{-(Q_D + E_b)}{RT}\right\} \qquad (4)$$

where k_0 and p_0 are constants, Q_D is the activation energy for diffusion, and E_b is the trap binding energy. The model has been used to analyse permeation test results [15], and TDS data [16–19]. Note, however, that there are a number of fitting parameters, k_0, p_0, E_b, N_t and this may be the reason why direct comparisons of calculations against experimental data have not been reported, but the model has been used to study qualitative trends [16–19].

2.3 Local Equilibrium

Oriani's model assumes that local equilibrium exists between the concentrations of hydrogen in the lattice and at traps, both for a static and dynamic population of hydrogen (i.e., during diffusion) and assuming no interactions between the occupied sites, [20]:

$$\frac{\theta_t(1 - \theta_l)}{\theta_l(1 - \theta_t)} = \exp\left\{\frac{E_b}{RT}\right\}. \qquad (5)$$

If both $\theta_t \ll 1$ and $\theta_l \ll 1$ then this equation simplifies to

$$C_t \approx \frac{N_t}{N_l} C_l \exp\left\{\frac{E_b}{RT}\right\}. \tag{6}$$

Since $N_t \ll N_l$, the cross–section available for diffusion is not significantly diminished by traps so the diffusion flux can be written in terms of just the lattice sites as

$$J = -D_l \frac{dC_l}{dz} \tag{7}$$

where D_l is the diffusivity of hydrogen in the undisturbed lattice. However, hydrogen at traps also contributes to the concentration gradient so an apparent diffusivity D_a can be defined such that

$$J = -D_a \frac{d(C_l + C_t)}{dz} \tag{8}$$

On comparing the diffusion coefficients in equations 7 and 8, and substituting the relationship between C_l and C_t from equation 6, it can be shown [20] that

$$D_a = D_l \frac{dC_l}{d(C_l + C_t)} = D_l \frac{C_l}{C_l + C_t(1 - \theta_t)} \approx \frac{D_l}{1 + \frac{N_t}{N_l} \exp\left\{\frac{E_b}{RT}\right\}} \tag{9}$$

with the approximation justified as long as $\theta_t \ll 1$. Note that the $(1 - \theta_t)$ term arises because there is no gradient in the concentration of traps if all traps are occupied.

Oriani's model has been applied extensively to extract the apparent diffusivity, trap density and binding energy from permeation experiments [15,21–24, for example]. It is, however, limited by the apparent diffusivity approach to dealing with the characteristics of just one kind of trap. The simplifying assumption $\theta_t \ll 1$ used to derive equation 9 is unlikely to be justified when dealing with TDS data on samples which are charged with significant concentrations of hydrogen. This is illustrated in Fig. 1 for a variety of binding energies; naturally, the approximation is particularly weak for high binding energies or large hydrogen concentrations. This might explain the poor agreement between experiment and theory reported by Yamaguchi and Nagumo when they applied the apparent diffusivity into a diffusion model to explain TDS results [25]; a further difficulty is that the apparent diffusivity, designed for isothermal conditions is applied to experiments involving continuous heating.

3 Numerical Analysis of Hydrogen Desorption

To cope with the limitations of the methods described above, a numerical finite difference method was programmed as described in Fig. 2. It is important to emphasise that the method permits multiple binding sites, here implemented for two trap sites with different binding energies. It is assumed that there is no interaction between the trapped and free hydrogen and that one-dimensional diffusion occurs through the lattice in a direction normal to the plane of a steel sheet. Hydrogen is first introduced into the sample and distributed between the trap sites and lattice sites either assuming local equilibrium or via a "kinetic model" based on the McNabb and Foster scheme. The lattice hydrogen is then allowed to diffuse out to the free surface using a finite difference method (FDM). This process is repeated until the sample reaches the target temperature.

Using symmetry it is only necessary to model half of the specimen, which for 1 mm length was divided into 50 elements after demonstrating that further subdivision did not make a significant difference to the calculated outcomes. In the case of austenite where diffusion is much slower, the number of elements per mm was increased to 800.

Hydrogen is first introduced into the sample assuming a constant surface concentration of 0.03 ppm, consistent with the extrapolated phase boundary of the Fe_α-H phase diagram [26]. The time interval was chosen to be less than $\frac{1}{3}(\Delta z)^2 D^{-1}$, where Δz is the dimension of the FDM element. The hydrogen that enters the steel was distributed between the trap sites and lattice sites either assuming local equilibrium or via a "kinetic model" based on the Mc-Nabb and Foster scheme. For the effusion part of the process which begins when charging is halted, the hydrogen concentration at the surface is set to zero, assuming that any interfacial reaction effects can be neglected [27], with diffusion through the lattice treated using the finite difference method, repeated until the sample reaches the target temperature. All of the hydrogen that leaves the sample during this stage comes from the escape of atoms from the trapping sites into the ferrite lattice.

The software for doing these calculations, together with examples of inputs and outputs, and documentation is available freely on:

http://www.msm.cam.ac.uk/map/steel/programs/hydrogen.html

3.1 Kinetic model

Here we adapt equation 3 to develop a kinetic model to represent concentrations within the steel. The chances ϕ_t and ϕ_d of the trapping or detrapping of hydrogen atoms will be related to the respective activation energies and the concentrations as follows:

$$\phi_t = \exp\left\{\frac{-Q_D}{RT}\right\} \frac{N_t(1-\theta_t)}{N_l(1-\theta_l) + N_t(1-\theta_t)}$$

$$\phi_d = \exp\left\{-\frac{(Q_D + E_b)}{RT}\right\} \frac{N_l(1-\theta_l)}{N_l(1-\theta_l) + N_t(1-\theta_t)}. \tag{10}$$

During a time interval dt, a hydrogen atom will make $\nu \times dt$ attempts at the activation barrier, where ν is an attempt frequency, here assumed to be the Debye frequency of $10^{13}\,\text{s}^{-1}$. It follows that probabilities p_t and p_d of the trapping and detrapping events are given by

$$p_t = 1 - (1 - \phi_t)^{dt\,\nu} \qquad \text{and} \qquad p_d = 1 - (1 - \phi_d)^{dt\,\nu} \tag{11}$$

so that the instantaneous concentrations C_l' and C_t' at the lattice and trap sites become:

$$C_l' = C_l(1 - p_t) + C_t\,p_d \qquad \text{and} \qquad C_t' = C_t(1 - p_d) + C_t\,p_t \tag{12}$$

after the time interval dt. These concentrations are adjusted during each time step of the numerical scheme, thus accounting explicitly for the barriers to the trapping or detrapping events.

3.2 Local equilibrium model

In contrast, a model based on the assumption of local equilibrium persisting at all stages of the calculation is simpler because the distribution of hydrogen atoms at lattice and trap sites is determined by making the chemical potential uniform, as in equation 6. However, in the present work, the approximation that $\theta_t \ll 1$ was avoided by using equation 5 instead, together with a mass conservation condition. This required the solution of the quadratic equation:

$$\exp(E_b/RT)N_l\theta_l^2 + \{\exp(E_b/RT)N_t + N_l\}\theta_l - (C_l + C_t) = 0 \tag{13}$$

to obtain the distribution of hydrogen on potential sites.

3.3   Comparison

The numerical model based on the kinetic and local equilibrium approaches, was utilised to study ferritic steel sheet-samples of $2\,\mathrm{mm}$ thickness, with heating rates of 100 and $200\,°\mathrm{C\,h^{-1}}$, a trap binding energy of $50\,\mathrm{kJ\,mol^{-1}}$ and lattice-site density $5.2{\times}10^{29}\,\mathrm{m^{-3}}$, trap density $2{\times}10^{24}\,\mathrm{m^{-3}}$. The diffusivity of hydrogen in ferrite was $D_0 = 5.8{\times}10^{-8}\,\mathrm{m^2\,s^{-1}}$ and $Q_D = 4.5\,\mathrm{kJ\,mol^{-1}}$ [28]. The densities are estimated as follows. There are six tetrahedral interstices which can accommodate hydrogen, per iron atom in ferrite, however it was assumed that only the half of total tetrahedral sites are active because of the known repulsion between near neighbour hydrogen pairs in ferrite [29]. Then

$$N_l = \frac{\text{Avogadro number}}{\text{molar volume}} \times 3 \qquad (14)$$

Dislocations and grain boundaries are the trap sites expected in annealed ferritic steel. The trap density due to dislocations was assumed as

$$N_t^\rho = \pi r_d^2 \rho N_l \qquad (15)$$

where r_d is is taken to be equal to b, the magnitude of the dislocation Burgers vector; this is consistent with previous work that the hydrogen is essentially trapped in the core of dislocation rather than in its extended strain field [30]. ρ is the dislocation density. The trap density due to grain boundaries was calculated as follows:

$$N_t^S = S_V r_d N_l \qquad (16)$$

where $r_d = 2b$, and S_V is the grain boundary surface area per unit volume. As an example, the trap density for a sample with a dislocation density of $10^{10}\,\mathrm{m^{-2}}$ and grain size $200\,\mathrm{\mu m}$, is about $2{\times}10^{24}\,\mathrm{m^{-3}}$ according to equations 15 and 16. It turns out that for the conditions studied, the results of the local equilibrium model and kinetic models are consistent, probably because the heating rate is not particularly large, so that an equilibrium distribution of hydrogen in maintained at all temperatures, Fig. 3.

4   Application

4.1   Experimental details

The aim was to measure the effect of the plastic strain on hydrogen desorption and to analyse the results with the numerical model. The chemical composition of the steel was

Fe-0.004C-0.078Mn-0.015Cr-0.046 Al-0.015 Ti wt%.

In order to reduce the effect from pre-existing dislocations and grain boundaries, the steel was heat treated at $950\,°C$ for $10\,min$ with heating and cooling rates of $\pm10\,°C\,s^{-1}$. Tensile test samples were then cut into $50\,mm$ guage length, $12.5\,mm$ width and $0.7\,mm$ thickness and plastically deformed to elongations of $10\,\%$ and $20\,\%$.

The specimens were then polished with 800 grit sand papers, and charged electrochemically with hydrogen for $12\,h$ using $3\,\%$ NaCl + $0.3\,\%$ NH$_4$SCN solution with $1\,A\,m^{-2}$. This charging period is sufficient to saturate the samples. TDS experiments started within $15\,min$ after the hydrogen charging was completed. The heating rate was 100 and $200\,°C\,h^{-1}$. The results were analysed at $3\,min$ intervals using helium as a carrier gas. The desorption rate was defined as the amount of hydrogen that evolves in $1\,min$. A standard mixture He + 10.2 volume ppm H$_2$ was used for calibrating the equipment.

Fig. 4a shows the microstructure after the heat treatment. The grain size was obtained as $120.3\pm19.6\,\mu m$ by using the lineal intercepts method. The Vickers hardness of the undeformed steel determined with a load of $1\,kg$ was $69\pm2\,HV1$. Fig. 4b shows the stress–strain curve. The dislocation density of the deformed steel was estimated by converting the tensile stress into a shear stress τ:

$$\tau = \tau_0 + \alpha G b\sqrt{\rho} \tag{17}$$

where α is a numerical constant with value of $0.3 - 0.6$, G is the shear modulus ($81.7\,GPa$) and b is the magnitude of the dislocation Burgers vector, equal to $0.287\,nm$ for ferrite. The calculated dislocation density changes for 10, $20\,\%$ deformed sample are 3.53×10^{13}, $6.31\times10^{13}\,m^{-2}$ with $\tau_0 = 48.5\,MPa$ (calculated as half the tensile stress at yielding in Fig. 4), $\alpha = 0.6$. It has been reported that for annealed iron, the measured dislocation density is practically zero when compared with that after implementation of plastic strains of the magnitudes considered here [31], so it has been assumed that the undeformed sample contains $\rho = 10^{10}\,m^{-2}$.

4.2 Hydrogen desorption analysis

The reversibility of hydrogen traps was investigated first. The charging and analysis were repeated three times with the maximum temperature on each occasion being $300\,°C$, but there was no significant change in the rate curves as shown in Fig. 5a. The desorption rates for the plastically strained samples are also shown at heating rates of 100 and $200\,°C\,h^{-1}$, respectively. The peak height increases with plastic strain, due presumably to the increasing dislocation density. The relation between the total hydrogen content and dislocation density is illustrated in Fig. 6. The hydrogen content was obtained from the area under the curve in Fig. 5 divided by the heating rate and considered as

8

a amount of hydrogen evolved after an interval of 15 min following hydrogen charging.

4.3 Prediction of desorption curves

Analysis of the data first requires values for the binding energies and trap densities. Assuming grain boundaries and dislocations as traps, equations 15 and 16 were used to calculate the number density of each trap as a function of the grain size and dislocation density derived from the tensile test data as explained previously. The binding energies for each of the trap sites was obtained by fitting to just one of the TDS curves, that of the 20% deformation sample heated at 100 °C h^{-1}. The resulting data are given in Table 1. The five remaining curves were predicted without altering the fitted values of the binding energies. The comparisons between experimental and calculated results are shown in Fig. 7. The total hydrogen evolution rate is from dislocations and grain boundaries, and their calculated individual contributions are illustrated in Fig. 8.

4.4 Application to literature data

There are published data on flat specimens, of the effect of plastic deformation on hydrogen desorption from interstitial-free steel with grain size 30 μm and thickness 2 mm. [32]. The results above 25 °C with the heating rate 100 °C h^{-1} are shown in Fig. 9. It is found that the data cannot be explained using the binding energies derived in the present work and the functions used to calculate trap densities, i.e., without fitting. However, the direct application of the present work is difficult because of a lack of the information about dislocation density and the fact that the hydrogen evolution occurs at a lower temperature than is the case in our experiments, even though the specimens used by Nagumo and co-workers are thicker. Furthermore, the maximum desorption rates are lower (cf. Fig. 5) in spite of the smaller 30 μm grain size reported for the sample studied. The reasons behind the discrepancies with our data are not clear.

There are further discrepancies when samples of pure iron are examined, where flat specimens heated at 60°C h^{-1} [30], and cylindrical pieces heated at 100°C h^{-1} [32] were studied. It was found that first hydrogen evolution peak in undeformed samples occurs at temperatures in the range 122-220°C, which are much greater than for the intersitial-free steel studied here, and indeed by Nagumo and co-workers [32]. The latter work was subsequently analysed using a numerical model by [19], but it was necessary to use a large binding energy of 61 kJ mol^{-1} in order to reproduce the approximate peak positions. This is a

reflection of the experimental data for annealed pure iron are dramatically inconsistent with those for interstitial free steel, in that the hydrogen is strongly trapped. The literature has not commented on these discrepancies, which also cannot be resolved by the use of the present model without changing fitting parameters.

It is also difficult to understand why in recent work, the TDS data for pure iron are insensitive to the amount of cold deformation [2]; it has been suggested that this is because the hydrogen is weakly bound to dislocations but this does not seem reasonable in the context of ferritic iron where the binding energy is believed widely to be greater than the activation energy for diffusion [33,15]. Previous work has concluded that in pure iron, much of the hydrogen is located at dislocations and that the amount of hydrogen scales significantly with the level of deformation [34,35]. Hagi and Hayashi [28] have tabulated data up to 1987, and in all cases the binding energy at dislocations is much greater than the activation energy for the diffusion of hydrogen. These data are all inconsistent with the experiments interpretation reported in [2].

Our intention in highlighting these discrepancies is to stimulate further work in the future. Whereas there are clear inconsistencies in reported experimental data, some of the reported variations, for example, in the binding energy of hydrogen at dislocations, some 20-60 kJ mol^{-1} [28] are undoubtedly due to approximations in the theoretical interpretations of the experimental data.

5   Theoretical Investigations

The numerical model described above was used to explore tendencies in TDS data, with concentration units in parts per million by weight (ppmw)[1]. The basis parameters used for the calculations include diffusivity as in [36], steel thickness $l = 2\,\mathrm{mm}$, $E_b = 50\,\mathrm{kJ\,mol^{-1}}$, $N_t = 2{\times}10^{24}\,\mathrm{m^{-3}}$, 100 °C h^{-1}; diffusible hydrogen was allowed to evolve for 20 min prior to the generation of the TDS curves. Calculations were conducted to see what effect variations in these parameters would have on the effusion of hydrogen from the sample.

Fig. 10 shows a variety of plots which illustrate trends. As might be expected from the longer diffusion distances, an increase in steel thickness causes more of the hydrogen to evolve at higher temperatures and extends the temperature range over which the effusion occurs. Stronger binding also shifts the TDS curves to greater temperatures, but it should be noted that the diffusion of hydrogen in ferrite has a much lower activation energy than the E_b values studied. The circumstances should be different for austenite where the activation

---

[1]   ppmw = $10^6\,N_l$/(density $\times$ Avogadros number)

energy for hydrogen diffusion is very large so the evolution rate should be less sensitive to trap binding energies. For example, the evolution rate of austenite was simulated with the condition of $l = 2\,\mathrm{mm}$, $N_l = 10^{29}\,\mathrm{m^{-3}}$, $\phi = 100\,^\circ\mathrm{C\,h^{-1}}$. A constant surface concentration of 0.08 ppm was used in this case, consistent with the extrapolated phase boundary of the Fe_γ-H phase diagram [26]. The diffusivity was used as $D_0 = 7 \times 10^{-8}\,\mathrm{m^2\,s^{-1}}$ and $\mathrm{Q}_D = 48\,\mathrm{kJ\,mol^{-1}}$ [37]. For the comparison, samples without traps and with traps that have a binding energy $30\,\mathrm{kJ\,mol^{-1}}$ and trap density $3 \times 10^{24}\,\mathrm{m^{-3}}$, were simulated. Fig. 11a shows the hydrogen profile after 72 h charging - as expected, the depth of hydrogen in the austenitic sample with traps is smaller when compared with that without traps. Note that the *total* concentration in the surface region of the sample with traps is greater than the solubility of hydrogen in austenite (0.08 ppm) because the hydrogen located at traps is included in the plot. Since the diffusivity of hydrogen in austenite is slow, the sample is not saturated even after 72 h of charging. The peak temperature is relatively insensitive to the presence or absence of traps because the controlling activation energy is that for diffusion, which is greater than the binding energy of the trap. However, the peak height is greater for the sample containing the traps because the total amount of hydrogen that can be absorbed into a sample with defects is naturally larger, Fig. 11b.

An interesting set of results is presented in Fig. 12, for multiple traps, a scenario which cannot be modelled by the apparent diffusivity approach which can only deal with a single TDS peak; the approach presented here can deal with arbitrary numbers of traps. The calculations use the following parameters: case 1 has traps with binding energies 40 and $55\,\mathrm{kJ\,mol^{-1}}$, with trap densities 5×10^{24} and $2 \times 10^{24}\,\mathrm{m^{-3}}$ respectively, with the other conditions are same as for the reference condition. The only difference with case 2 is that the binding energies are changed to 47 and $50\,\mathrm{kJ\,mol^{-1}}$.

Fig. 12a shows that for the conditions studied, a relatively large difference in the binding energies of the two kinds of traps leads to a curve (case 1) in which hydrogen evolution effectively occurs in two stages, whereas a smaller difference leads to overlap of the detrapping events from the two traps and hence an apparently simple peak shape. This interpretation is confirmed from the plot (Fig. 12b) of the hydrogen concentrations at different locations within the specimen. Fig. 12b, the lattice hydrogen comes entirely from detrapping from the two defects which bind the hydrogen. The hydrogen from the less potent trap is exhausted by about 100°C so that the major contribution to the lattice hydrogen then comes from the trap with the largest binding energy, and this is reflected in the shape of the lattice hydrogen curve.

11

6   Summary and Conclusions

The measurement of hydrogen evolution rates from samples of steel is relatively simple, and the rigorous interpretation of the results can in principle lead to the better design of steels, for example, by manipulating trap densities. In fact, this forms the basis of steels designed to strongly trap nascent hydrogen so that they become less susceptible to phenomena such as static fracture. However, there are well understood difficulties and approximations in the simple application of analytical models to thermal desorption spectra, which are mitigated by using the finite difference technique which embodies the well-known kinetic and thermodynamic principles. Such a model has been created, and it avoids common approximations such as the assumption that fraction of traps occupied is much smaller than unity, and that there the hydrogen is captured by just one variety of trap. Furthermore, the source code and documentation for the analysis are freely available and we hope will form the basis for generic comparisons with experimental TDS data.

The following conclusions can be reached from the present work, based on the study of a simple steel microstructure which should contain only grain boundaries and dislocations as significant traps:

- the binding energies for hydrogen trapped at ferrite-ferrite grain boundaries and at dislocations were derived to be 49 and $44\,\mathrm{kJ\,mol^{-1}}$, respectively. These are reasonable values when compared with independent data listed in, for example, [33], and with the general observation from single and polycrystalline samples that boundaries are stronger traps [30]. In addition, the avoidance of common approximations in the interpretation of desorption spectra should make these values more meaningful so that in future they are not treated as fitting parameters. The fact that the binding energy is greater at grain boundaries might be expected because of their more open structure relative to line defects.

- The binding energies were obtained by fitting to just one desorption curve, and were able to predict another five sets of data. However, unexplained discrepancies have been noted with published data [32] which show much smaller desorption rates in spite of greater trap densities and thicker samples.

- Functions have been derived to represent the number density of traps at grain boundaries and dislocations. The functions are physically based and the method in principle removes two fitting parameters common in TDS analysis.

- It has been possible to deal simultaneously with two traps, and to calculate

the contributions of each of these traps to the total hydrogen evolved. The method is in principle not limited to just two traps and will be extended in the future to include carbides and other phases such as retained austenite.

- Finally, there are significant, unresolved discrepancies in published observations of hydrogen desorption from pure iron as compared with that from interstitial-free iron. In particular, it is not clear why the trapping seems to be much stronger in the former case, when assessed from the elevation of desorption rate peaks to higher temperatures.

References

[1] J. H. Ryu, Y. S. Chun, C. S. Lee, H. K. D. H. Bhadeshia, and D. W. Suh. Effect of deformation on hydrogen trapping and effusion in TRIP-assisted steel. *Acta Materialia*, 60:4085–4092, 2012.

[2] D. Pérez Escobar, T. Depover, L. Duprez, K. Verbeken, and M. Verhaege. Combined thermal desorption spectroscopy, differential scanning calorimetry, scanning electron microscopy and x-ray diffraction study of hydrogen trapping in cold deformed trip steel. *Acta Materialia*, 60:2593–2605, 2012.

[3] J. Takahashi, K. Kawakami, and M. Ueda. Atom probe tomography analysis of the white etching layer in a rail track surface. *Acta Materialia*, 58:3602–3612, 2010.

[4] Y. Hagihara, T. Shobu, N. Hisamori, H. Suzuki, K. Takai, and K. Hirai. Delayed fracture uing CSRT and hydrogen trapping characterisitics of V–bearing hihg–strength steel. *ISIJ International*, 52:298–306, 2012.

[5] L. S. Darken and R. P. Smith. Behaviour of hydrogen in steel during and after immersion in acid. *Corrosion*, 5:1–16, 1949.

[6] H. E. Kissinger. Reaction kinetics in differential thermal analysis. *Analytical Chemistry*, 29:1702–1706, 1957.

[7] A. Cornish-Bowden. *Fundamentals of Enzyme Kinetics*. Wiley-VCH Verlag GmbH & Co., Berlin, Germany, 2012.

[8] W. Y. Choo and J. Y. Lee. Thermal analysis of trapped hydrogen in pure iron. *Metallurgical Transactions A*, 13:135–140, 1982.

[9] J. Y. Lee and S. M. Lee. Hydrogen trapping phenomena in metals with b.c.c. and f.c.c. crystal structures by the desorption thermal analysis technique. *Surface and Coatings Technology*, 28:301–314, 1986.

[10] K. Takai and R. Watanuki. Hydrogen in trapping states innocuous to environmental degradation of high-strength steels. *ISIJ International*, 43:520–526, 2003.

[11] F. G. Wei and K. Tsuzaki. Quantitative analysis on hydrogen trapping of TiC particles in steel. *Metallurgical & Materials Transactions A*, 37:331–353, 2006.

[12] M. Wang, E. Akiyama, and K. Tsuzaki. Effect of hydrogenslow on the fracture behavior of high strength steel during slow strain rate test. *Corrosion Science*, 49:4081–4097, 2007.

[13] A. McNabb and P. K. Foster. A new analysis of the diffusion of hydrogen in iron and ferritic steels. *Trans. AIME*, 227:618–627, 1963.

[14] G. R. Caskey and W. L. Pillinger. Effect of trapping on hydrogen permeation. *Metallurgical and Materials Transactions A*, pages 467–476, 1975.

[15] A. J. Kumnick and H. H. Johnson. Deep trapping states for hydrogen in deformed iron. *Acta Metallurgica*, 28:33–39, 1980.

[16] K. L. Wilson and M. I. Baskes. Deuterium trapping in irradiated 316 stainless steel. *Journal of Nuclear Materials*, 76–77:291–297, 1978.

[17] A. Turnbull, R. B. Hutchings, and D. H. Ferriss. Modelling of thermal desorption of hydrogen from metals. *Materials Science & Engineering A*, 238:317–328, 1997.

[18] M. Enomoto, D. Hirakami, and T. Tarui. Modeling thermal desorption analysis of hydrogen in steel. *ISIJ International*, 46:1381–1387, 2006.

[19] K. Ebihara, T. Suzudo, H. Kaburaki, K. Takai, and S. Takebayashi. Modeling of hydrogen thermal desorption profile of pure iron and eutectoid steel. *ISIJ International*, 47:1131–1140, 2007.

[20] R. A. Oriani. The diffusion and trapping of hydrogen in steel. *Acta Metallurgica*, 18:147–157, 1970.

[21] Y. Mine, Z. Horita, and Y. Murakami. Effect of high-pressure torsion on hydrogen trapping in Fe-0.01 mass% C and type 310S austenitic stainless steel. *Acta Materialia*, 58:649–657, 2010.

[22] S. Frappart, A. Oudriss, X. Feaugas, J. Creus, J. Bouhattate, F. Thébault, L. Delattre, and H. Marchbois. Hydrogen trapping in martensitic steel investigated using electrochemical permeation and thermal desorption spectroscopy. *Scripta Materialia*, 65:859–862, 2011.

[23] A. Oudriss, J. Creus, J. Bouhattate, E. Conforto, C. Berziou, C. Savall, and X. feaugas. Grain size and grain-boundary effects on diffusion and trapping of hydrogen in pure nickel. *Acta Materialia*, 60:6814–6828, 2012.

[24] J. Svoboda and F. D. Fisher. Modelling for hydrogen diffusion in metals with traps revisited. *Acta Materialia*, 60:1211–1220, 2012.

[25] T. Yamaguchi and M. Nagumo. Simulation of hydrogen thermal desorption under reversible trapping by lattice defects. *ISIJ International*, 43:514–519, 2003.

[26] A San-Martin and FD Manchester. The fe-h (iron-hydrogen) system. *Journal of Phase Equilibria*, 11:173–184, 1990.

[27] B. Klemit, S. Köhle, K. P. Johann, A. Jungrethmeier, and J. Molinero. Dynamic process model for denitrogenation and dehydrogenation by vacuum degassing. *Scandanavian Journal of Metallurgy*, 29:194–205, 2000.

[28] H. Hagi and Y. Hayashi. Effect of dislocation trapping on hydrogen and deuterium diffusion in iron. *Trans. JIM*, 28:368–374, 1987.

[29] C. Minot and C. Demangeat. Binding energy of a pair of hydrogen atoms in α-iron. *Physics Letters A*, 108:285–288, 1985.

[30] K. Ono and M. Meshii. Hydrogen detrapping from grain boundaries and dislocations in high purity iron. *Acta Metallurgica et Materalia*, 40:1357–1364, 1992.

[31] H. Hagi and Y. Hayashi. Effects of interstitial impurities on dislocation trapping of hydrogen in iron. *Trans. JIM*, 28:375–382, 1987.

[32] M. Nagumo, K. Takai, and N. Okuda. Nature of hydrogen trapping sites in steels induced by plastic deformation. *Journal of Alloys and Compounds*, 293–295:310–316, 1999.

[33] J. P. Hirth. Effects of hydrogen on the properties of iron and steel. *Metallurgical & Materials Transactions A*, 11(861–890), 1980.

[34] C. M Sururges and A. P. Miodownik. The interaction of hydrogen and dislocations in iron. *Acta Metallurgica*, 17:1197–1207, 1969.

[35] G. W. Hong and J. Y. Lee. The interaction of hydrogen with dislocation in iron. *Acta Metallurgica*, 32:1581–1589, 1984.

[36] H. Hagi. Diffusion coefficient of hydrogen in iron without trapping by dislocations and impurities. *Materials Transactions, JIM*, 35:112–112, 1994.

[37] S. Xiukui, X. Jian, and L. Yiyi. Hydrogen permeation behaviour in austenitic stainless steels. *Materials Science & Engineering A*, 114:179–187, 1989.
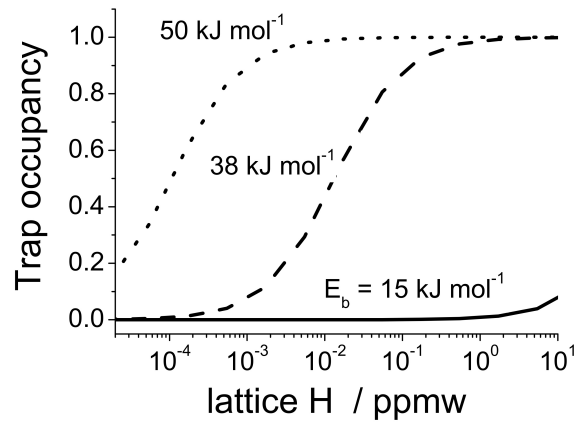
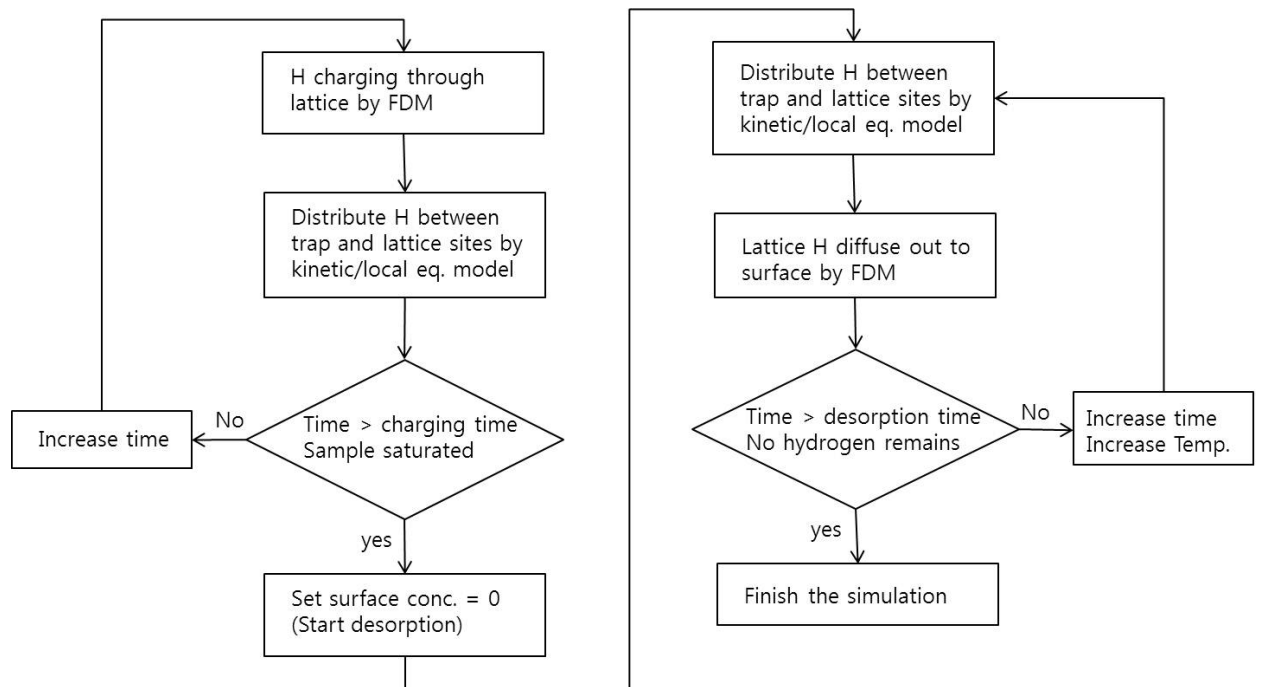Fig. 1. Trap occupancy as a function of hydrogen content at 300 K.

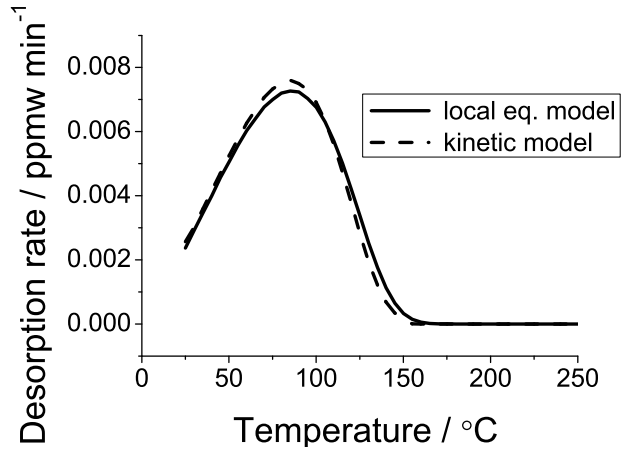Fig. 2. Flow chart illustrating the numerical calculation process.

16

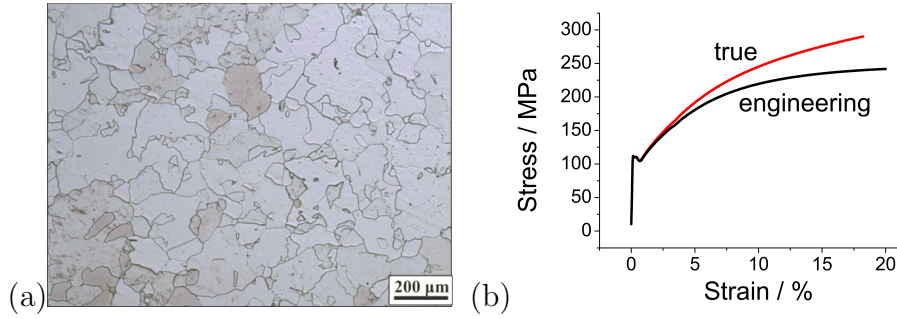Fig. 3. The results using both local equilibrium and kinetic models.

Fig. 4. (a) Sample after heat treatment at 950°C for 10 min, (b) strain–stress curves.

Table 1
Parameters used to calculate the TDS results with different plastic strain. Two kinds of traps, grain boundary and dislocation were assumed to exist. The diffusivity data are from [28].

	0%	10%	20%
N_t^S (10^{24} m^{-3})	2.49	2.49	2.49
E_S (kJ mol^{-1})	49	49	49
N_t^ρ (10^{24} m^{-3})	0.0007	2.37	4.25
E_ρ (kJ mol^{-1})	44	44	44
D_0 (10^{-8} m^2 s^{-1})	5.8	5.8	5.8
Q_D (kJ mol^{-1})	4.5	4.5	4.5

(a)

(b)
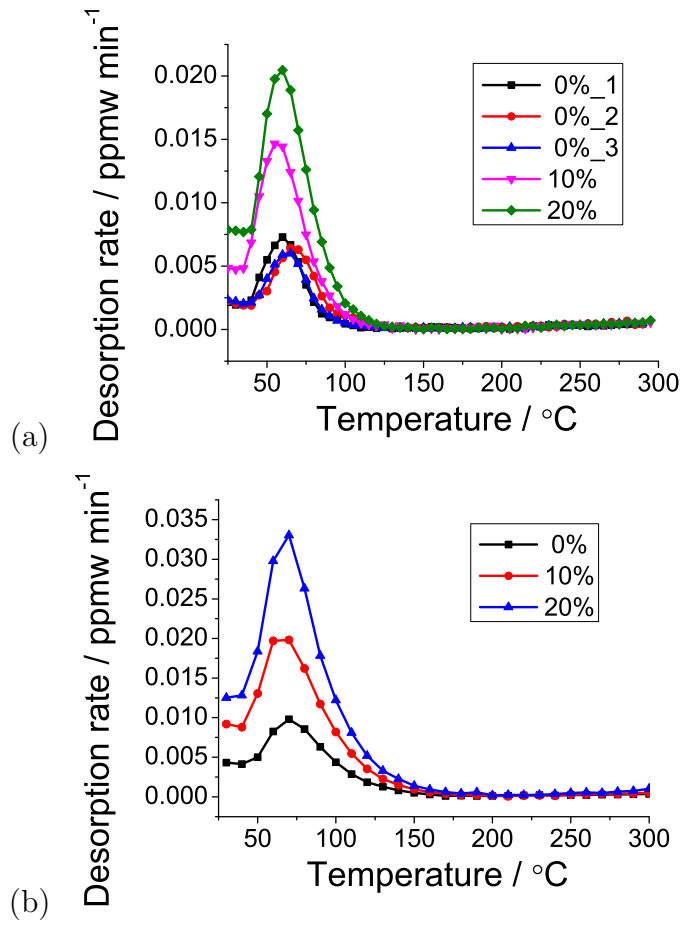
Fig. 5. Measured TDS data for heating rates of (a) $100\,^\circ\mathrm{C}\,\mathrm{h}^{-1}$ and (b) $200\,^\circ\mathrm{C}\,\mathrm{h}^{-1}$
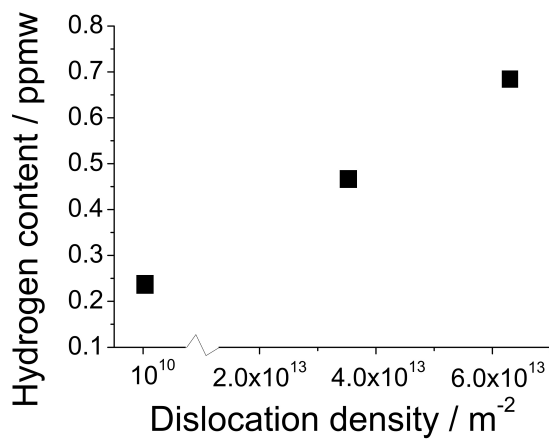
Fig. 6. Total hydrogen content as a function of the dislocation density.
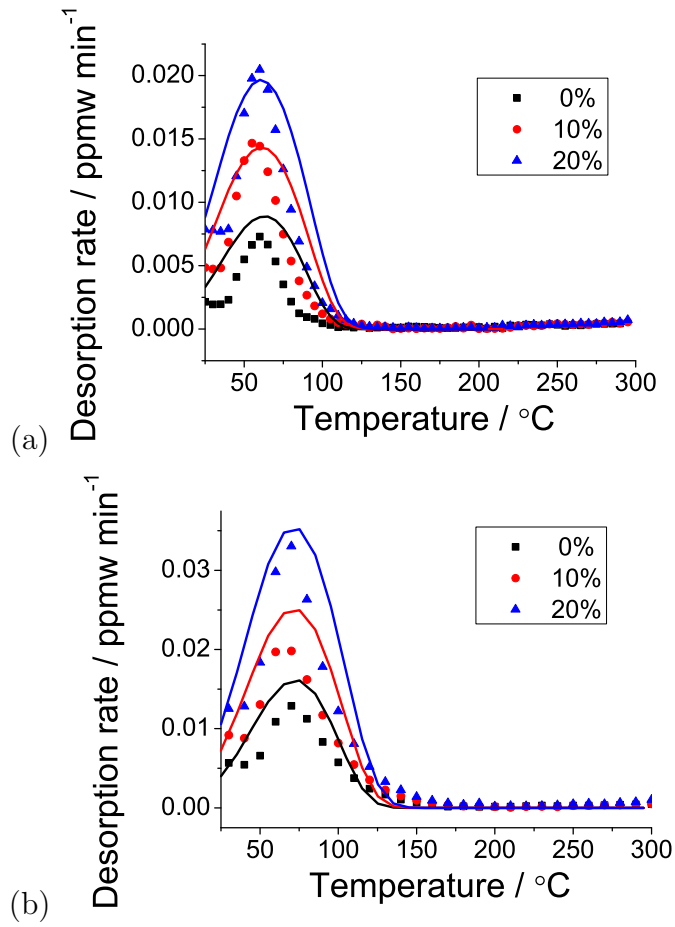
(a)

(b)

Fig. 7. Comparisons between experimental (points) and calculated (curves) results for the heating rates (a) $100\,^{\circ}\mathrm{C}\,\mathrm{h}^{-1}$ and (b) $200\,^{\circ}\mathrm{C}\,\mathrm{h}^{-1}$
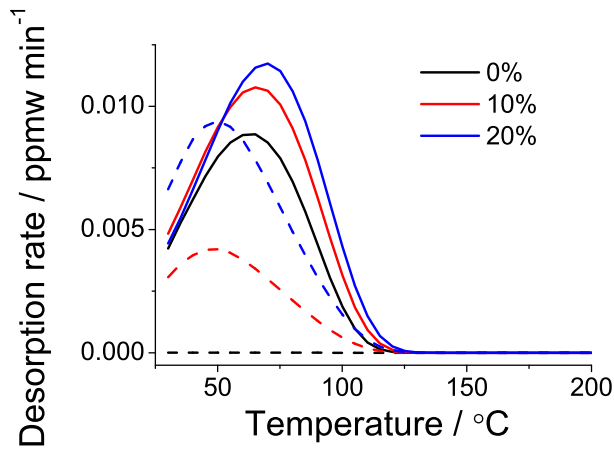
Fig. 8. Calculated TDS curves for hydrogen emanating from individual traps for a heating rate of $100\,^{\circ}\mathrm{C}\,\mathrm{h}^{-1}$. The solid and dashed line indicate the H desorption rate from grain boundary and dislocation respectively.
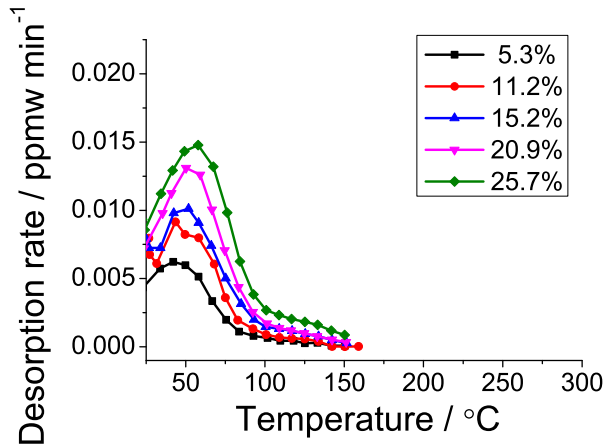
19

Fig. 9. Reported TDS data for interstitial-free steel [32].
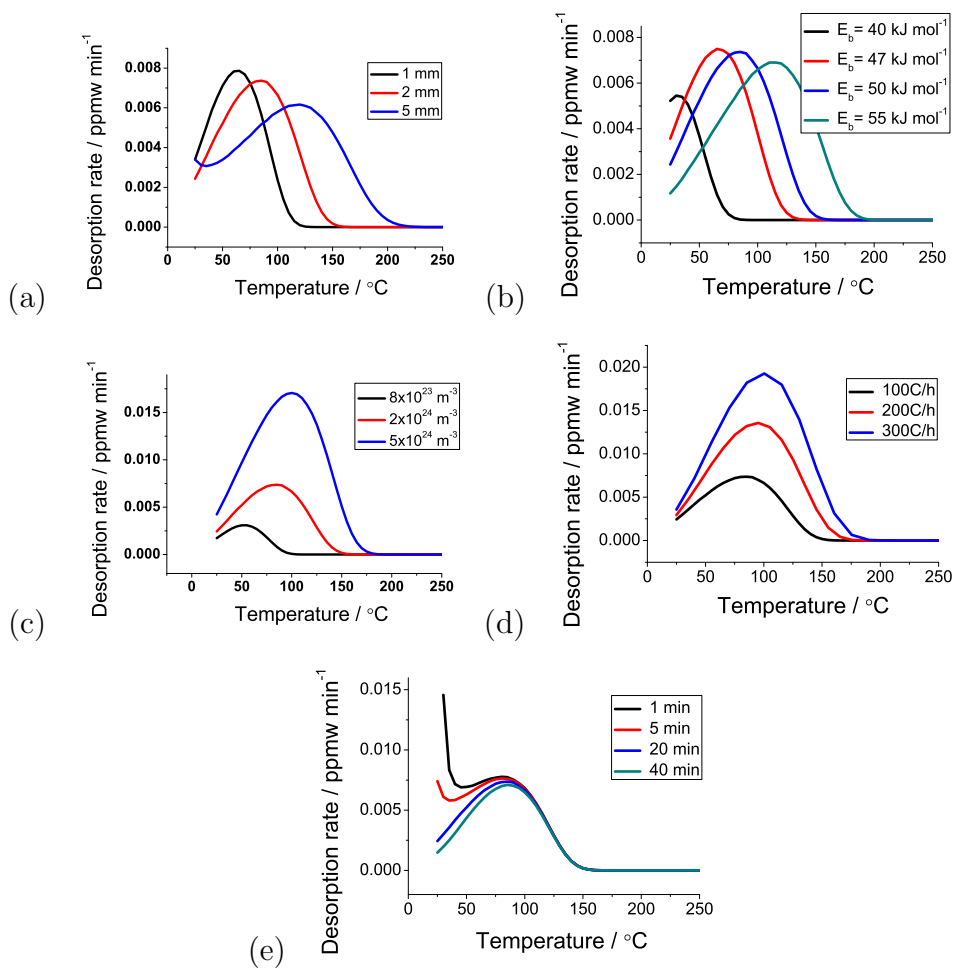

Fig. 10. Calculated TDS curves as a function of (a) sample thickness, (b) binding energy and (c) trap density (d) heating rate and (e) room temperature aging time. Note that the area under each curve, divided by the heating rate represents the total hydrogen content effused for the relevant temperature interval.
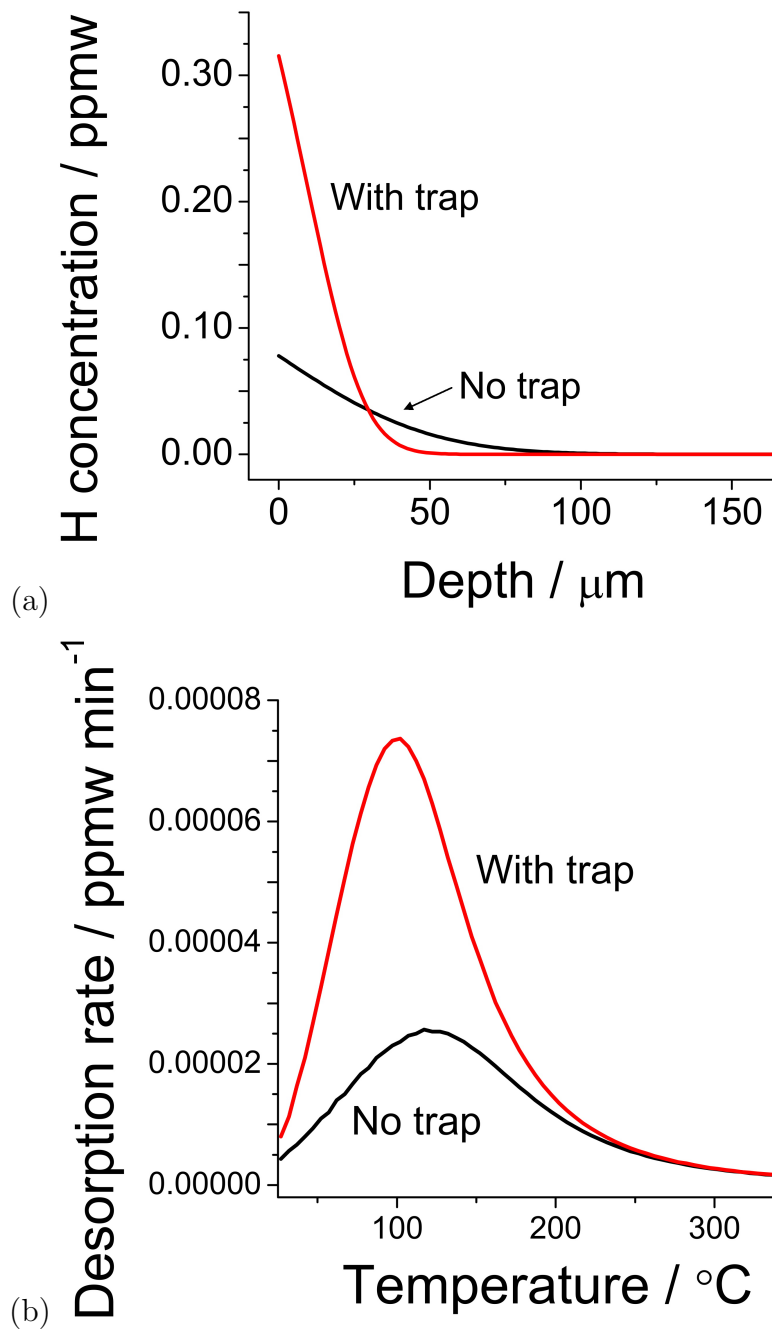
(a)

(b)

Fig. 11. Calculated (a) Total hydrogen content (lattice and traps) following 72 h of charging and (b) calculated TDS results.
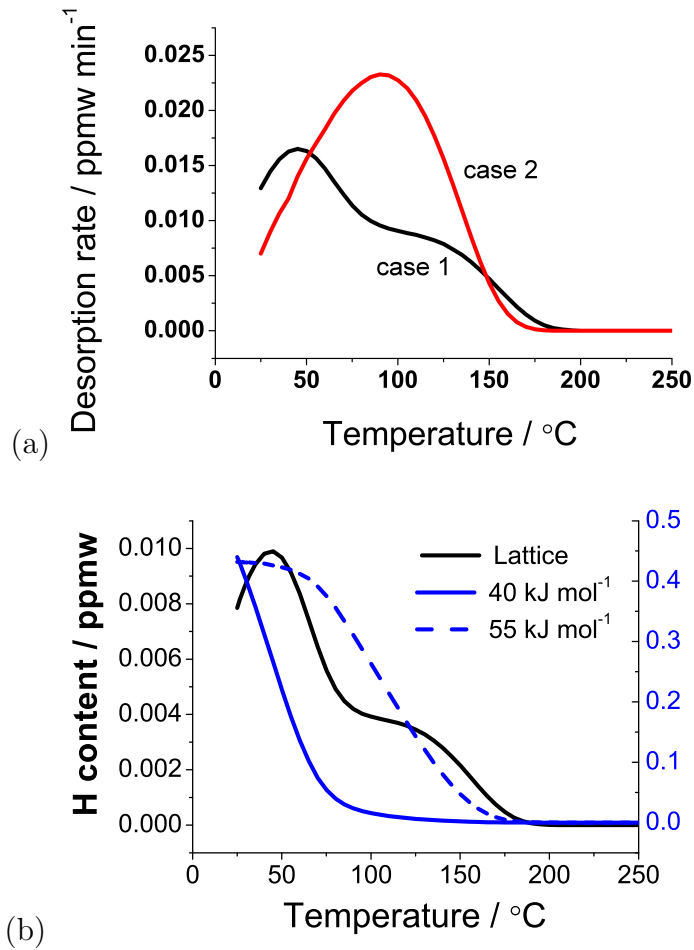
(a)

(b)

Fig. 12. Calculated TDS results when two different trapping sites are present; case 1 is when binding energy difference is large, whereas the other case involves binding energies with smaller difference. (b) Calculated profile for case 1. The vertical scale on the left hand side refers to lattice hydrogen and that on the right to trapped hydrogen.